Atomistic simulations of electric field effects on the Young's modulus of metal nanowires

2014 Nanotechnology 25 455704

(http://iopscience.iop.org/0957-4484/25/45/455704)

IOP Publishing Nanotechnology
Nanotechnology **25** (2014) 455704 (7pp) doi:10.1088/0957-4484/25/45/455704

Atomistic simulations of electric field effects on the Young's modulus of metal nanowires

Xue Ben and Harold S Park

Department of Mechanical Engineering, Boston University, Boston, MA 02215, USA

E-mail: xueben@bu.edu and parkhs@bu.edu

Received 13 July 2014, revised 16 September 2014
Accepted for publication 1 October 2014
Published 22 October 2014

Abstract

We present a computational, atomistic study of electric field effects on the Young's modulus of metal nanowires. The simulations are electromechanically coupled, where the mechanical forces on the atoms are obtained from realistic embedded atom method potentials, and where the electrostatic forces on the atoms are obtained using a point dipole electrostatic model that is modified to account for the different polarizability and bonding environment of surface atoms. By considering three different nanowire axial orientations (⟨100⟩, ⟨110⟩ and ⟨111⟩) of varying cross sectional sizes and aspect ratios, we find that the Young's modulus of the nanowires differs from that predicted for the purely mechanical case due to the elimination of nonlinear elastic stiffening or softening effects due to the electric field-induced positive relaxation strain relative to the relaxed mechanical configuration. We further find that ⟨100⟩ nanowires are most sensitive to the applied electric field, with Young's moduli that can be increased more than 20% with increasing aspect ratio. Finally, while the orientation of the transverse surfaces does impact the Young's modulus of the nanowires under applied electric field, the key factor controlling the magnitude of the stiffness change of the nanowires is the distance between atomic planes along the axial direction of the nanowire bulk.

Keywords: nanowire, electric field, Young's modulus

(Some figures may appear in colour only in the online journal)

1. Introduction

Low dimensional materials such as nanowires are known due to their large surface area to volume ratio to exhibit unique electronic, thermal, optical and mechanical properties as compared to standard bulk materials [1–3]. These physical properties have motivated the usage of nanowires as a potential building block for future nanotechnologies [4, 5] and nanoelectromechanical systems (NEMS) [6–8]. In many of these applications, particularly for NEMS, the nanowire is actuated by an externally applied electric field [9]. For example, the elastic properties of nanowires are often obtained by *in situ* transmission electron microscopy (TEM), in which the mechanical resonance of the nanowire is induced by the electrostatic forces that result from an alternating voltage [10–13].

However, when a conductive nanowire is subject to an electric field, its surface must be charged and polarized, and so there will be electrostatic forces exerted on the nanowire. When an electrostatic field is applied, researchers have reported that the pressure on the nanowire surface is negative due to the strong electrostatic force when the distance between the nanowire and the electrode is small [9]. Because of this, it is natural to wonder whether the electric field applied by the *in situ* TEM has any influence on the measured Young's modulus of the nanowire.

This question of electric field-induced effects on the elastic properties of nanostructures has driven research by various groups, though the majority of the existing work has been done on carbon nanotubes [14, 15]. In contrast, the effects of static electric fields on the Young's modulus of metal nanowires have not been studied extensively [16]. For example, Zhu *et al* used a continuum surface elastic theory that accounted for electric field effects by incorporating it into the surface energy, and derived analytic expressions for the effective Young's modulus [16], finding that the electric field had a stronger effect with decreasing nanowire cross sectional dimension.

However, previous studies on metal nanowire/electric field interactions have not used a realistic atomistic model that accounts for surface orientation, axial orientation, and surface and bulk polarization in determining the Young's modulus. Our work thus presents new insights on the role of electric field effects on the elastic properties of fcc metal nanowires resulting from coupled electromechanical atomistic calculations.

2. Methodology

The physical phenomena that must be captured for the electric field-induced coupling with the mechanical behavior involves accounting for the dipolar forces that arise for each atom in a metallic nanostructure due to the externally applied electric field. These induced dipoles result in an electrostatic force that will either augment or oppose any mechanical force that is applied to probe the mechanical properties of the nanostructure [17, 18].

To formally study this coupled electromechanical problem, we write the total system energy of the nanostructure as the sum of the mechanical and electrostatic energies as [19, 20]

$$V^{\text{total}}(r_{ij}) = \sum_{i=1}^{N}\sum_{j=1}^{N} V_{ij}^{\text{elec}}(r_{ij}) + \sum_{i=1}^{N}\sum_{j=1}^{N} V_{ij}^{\text{mech}}(r_{ij}), \tag{1}$$

where N is the total number of atoms in the system and r_{ij} is the distance between atoms i and j. The mechanical potential energy V^{mech}, and the resulting interatomic forces for silver is obtained using the well-established embedded atom (EAM) potential [21], which is known to accurately represent both the bulk and surface properties for transition fcc metals [23].

The calculation of the electrostatic forces is less standard, and so we present it in further detail here. In this model, based on the formulation of Jensen and Jensen [24], we account for these polarization-induced forces using a modification of classical electrostatics, in which we associate an atomic polarizability with each atom and calculate the induced dipole for each atom self-consistently through their interactions with each other as well as the externally applied electric field using the relationships of classical electrostatics [24].

For the nanowires we study, there are no net charges and chemical potential, so the total electrostatic energy V of the nanosystem can be written as

$$V = -\frac{1}{2}\sum_{i}^{N}\sum_{j}^{N} \mu_{i,\alpha}^{\text{ind}} T_{ij,\alpha\beta}^{11} \mu_{j,\beta}^{\text{ind}} - \sum_{i}^{N} E_{i,\alpha}^{\text{ext}} \mu_{i,\alpha}^{\text{ind}}, \tag{2}$$

where for nanowires in vacuum, the dipole–dipole interaction tensor $T_{ij,\alpha\beta}^{11}$ is derived from classical electrostatics [24], E^{ext} is the external electric field, and μ is the dipole associated with each atom.

The dipole for each atom is obtained self-consistently by taking the derivative of equation (2) with respect to the induced dipole μ^{ind}, giving the following set of linear equations

$$\begin{aligned}\left(\mu^{\text{ind}}\right) &= \left(\left(T^{11}\right)_{3N\times 3N}\right)^{-1}\left(-E^{\text{ext}}\right)\\ &= (T)^{-1}\left(-E^{\text{ext}}\right).\end{aligned} \tag{3}$$

Once the induced dipole on each atom is obtained from (3), the total electrostatic energy of the system is written as

$$V = -\frac{1}{2}\sum_{i}^{N} E_{i,\alpha}^{\text{ext}} \cdot \mu_{i,\alpha}^{*}, \tag{4}$$

where μ^* is the solution of μ^{ind} from (3). The electrostatic force $\vec{F}_k^{\text{elec}}$ on each atom k can be obtained by differentiating the electrostatic total energy in (4) with respect to the atom positions to yield

$$\begin{aligned}\vec{F}_k^{\text{elec}} &= -\nabla_k V\\ &= -\nabla_k\left[-\frac{1}{2}\sum_{i}^{N}\vec{E}_i^{\text{ext}}\cdot\vec{\mu}_i^{*}\right]\\ &= \frac{1}{2}\sum_{i}^{N}\left(\nabla_k\otimes\vec{\mu}_i^{*}\right)\vec{E}_i^{\text{ext}}\\ &\quad + \frac{1}{2}\sum_{i}^{N}\left(\nabla_k\otimes\vec{E}_k^{\text{ext}}\right)\vec{\mu}_k^{*}.\end{aligned} \tag{5}$$

A key modification to the atomistic electrostatic model presented above is to account for discrete nanoscale surface effects, where atoms that lie at corners, surfaces and edges have a different coordination number (i.e. number of bonding neighbors) than do bulk atoms, which will impact their dielectric response and dipolar polarizability. We capture these effects in the present work by adopting the method first proposed by Payton *et al* [25].

To do so, we note that in classical electrodynamic theory, the Clausius–Mossotti relation defines the polarizability α as

$$\alpha = \frac{3V}{4\pi}\frac{\epsilon-\epsilon_0}{\epsilon+2\epsilon_0}, \tag{6}$$

where V is the effective volume of the atom, ϵ is the dielectric constant of silver, ϵ_0 is the dielectric constant of the environment, and the cubic volume $V = 8R^3$. So

$$\alpha = \frac{6}{\pi}R^3\frac{\epsilon-\epsilon_0}{\epsilon+2\epsilon_0}, \tag{7}$$

where the effective radius for each atom is given by

$$R = R_{\text{surf}}(1-X) + XR_{\text{bulk}}, \tag{8}$$

where

$$X = \frac{\text{MIN}\left(\text{CN}_m, \text{CN}_{\text{max}}\right)}{\text{CN}_{\text{max}}}, \tag{9}$$

here $\text{CN}_{\text{max}} = 12$ is the maximum coordination number for an fcc atom, and CN_m is the effective coordination number for

atom m, calculated as

$$\mathrm{CN}_m = \sum_{n \neq m}^{N} f_c\left(\left|r_{mn}\right|\right), \tag{10}$$

where

$$f_c\left(\left|r_{mn}\right|\right) = \begin{cases} 1 & \text{if} |r_{mn}| < |r_{\min}| \\ \frac{1}{2}\left(1 + \cos\frac{\pi\left|r_{mn}\right|}{\left|r_{\max}\right| - \left|r_{\min}\right|}\right) & \text{if} |r_{\min}| \leqq |r_{mn}| \leqq |r_{\max}| \\ 0 & \text{if} |r_{mn}| > |r_{\min}| \end{cases}$$

which connects the atoms inside and outside of the coordination sphere smoothly, while accounting for variations from the standard bulk coordination number of 12. The specific parameters we utilized are $R_{\mathrm{surf}} = 1.65$ Å, $R_{\mathrm{bulk}} = 1.56$ Å, $r_{\min} = 3.0$ Å, $r_{\max} = 5.0$ Å, $\epsilon_0 = 1.0$. Furthermore, for electrostatic problems, the dielectric constant is infinite, so the polarizability can be simplified as $\alpha = \frac{6}{\pi}R^3$. Finally, we note that this atomistic electrostatic model is conceptually similar as the well-known discrete dipole approximation [26], with the key differences that each dipole is associated with an atom rather than an arbitrary volume, along with the fact that each atom has a position-dependent effective radius, therefore position-dependent polarizability.

As discussed above, the electrostatic forces are obtained based on (5) with the dielectric constant for silver obtained from the experimental work of Johnson and Christy [27], while the mechanical forces are obtained using the EAM potential for silver [21]. To implement this electromechanical coupling, the electrostatic forces were implemented in a standalone function that was called and used to augment the mechanical force during each conjugate gradient iteration performed by the open source LAMMPS [28] atomistic simulation code.

3. Simulation description

The simulations were performed as follows. First, silver nanowires of various sizes, surface orientations, axial orientations and aspect ratios were created with the atoms placed at the bulk lattice spacing for silver of 4.09 Å. The nanowires were then relaxed to their equilibrium configurations without any applied electric field subject to the boundary condition that the atoms lying in the outermost planes at each end of the nanowire are constrained to move axially along the nanowire length. During this relaxation process, the nanowires contract in length due to the presence of tensile surface stresses [29–31]. After mechanical relaxation, the equilibrium configuration for a given electric field intensity is found by gradually increasing the electric field in small increments up to the specified value, while finding the equilibrium configuration of the nanowire for each electric field increment while again constraining the atoms that lie in the planes at each end of the nanowire to move in the axial direction. Increasing the intensity of the electric field results in an expansion of the nanowire due to the induced dipole–dipole repulsion.

Once this electromechanical equilibrium was found, the nanowires were deformed uniaxially in tension and compression by fixing the two ends of the nanowire, and applying strain in increments of 0.025% while the constant electric field continued to be applied. The Young's modulus of the nanowire was calculated by extracting the reaction force at the displaced ends, and then converting it to stress by normalizing by the nanowire cross sectional area, and calculating the slope of the resulting stress versus strain curve.

We studied four different types of silver nanowires. We first studied ⟨100⟩/{100} nanowires and ⟨100⟩/{110} nanowires. Because these have the same ⟨100⟩ axial orientation, this will enable us to determine what effect different transverse surface orientations have on the electromechanical coupling. To study different axial orientations, we also studied ⟨110⟩ and ⟨111⟩ oriented silver nanowires. The cross sectional lengths D we considered were typically about $2 \times 2\ \mathrm{nm}^2$, while the nanowire lengths L were chosen such as aspect ratios L/D from 2 up to 5 were considered. Finally, electric field values of 0.1, 0.2 and 0.3 V Å^{-1} were applied to the nanowires. These values were chosen due to being commonly used in *in situ* TEM [19].

4. Effects of electrostatic field on nanowire Young's modulus

4.1. Relaxation strain

Before characterizing the electric field effects on the elastic properties of the nanowires, we first characterize the relaxation strain for ⟨100⟩/{100} nanowires with cross sectional length of $D = 2$ nm, and axial length from 4 to 10 nm, or aspect ratio L/D ranging from 2–5. This is done as representative trends, such as the sensitivity of the nanowires to applied electric fields for different aspect ratios and electric field strengths, can be gleaned.

The results are shown in figure 1. Specifically, it is clear that as the electric field intensity increases, so does the tensile relaxation strain, where we note that the strain is calculated with respect to the mechanically relaxed configuration, where the nanowire length is shorter than if the atoms sit at the bulk lattice sites due to the compressive strain induced by the tensile surface stresses [30]. The elongation of the nanowire relative to the mechanically relaxed configuration occurs due to the large tensile electrostatic forces that result at the two ends of the nanowires as a result of the applied electric fields, which cause elongation of the nanowire as compared to the nanowires that contract due to mechanical surface stresses.

Figure 1 also shows that the relaxation strain depends on the nanowire aspect ratio L/D. As can be seen, for a given electric field intensity, the tensile relaxation strain is largest for the largest aspect ratio nanowire of $L/D = 5$, or when $L = 10$ nm. We also note that the deformation of the nanowire is the same if the electric field direction is reversed, which is

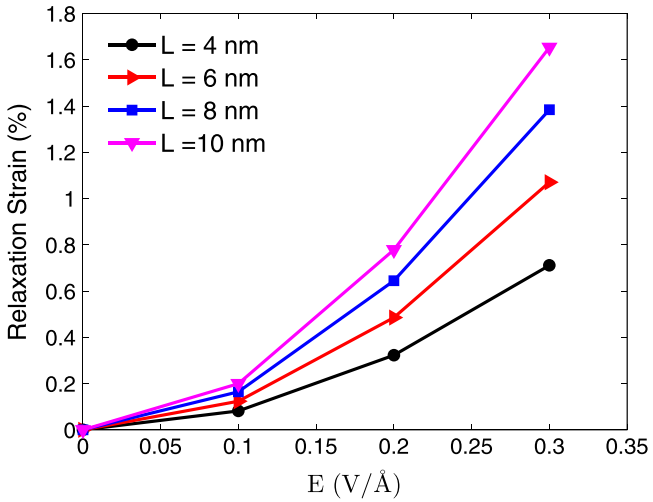

Figure 1. The relaxation strain versus electric field intensity for a 2 nm side length ⟨100⟩/{100} nanowire, and the nanowire axial length varies from 4 to 10 nm, or the aspect ratio of the nanowire ranges from 2 to 5.

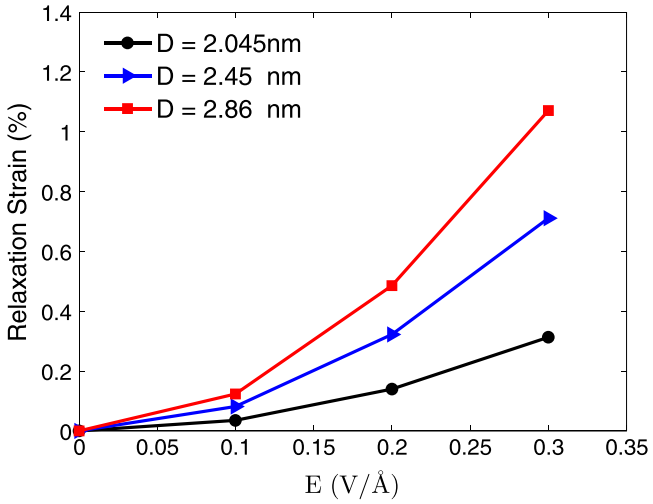

Figure 2. The relaxation strain versus electric field intensity for a 6 nm axial length ⟨100⟩/{100} nanowire where the nanowire side length varies from 2 nm to around 3 nm.

similar to previous results obtained for electrostatically actuated carbon nanotubes [18].

Because figure 1 considered a constant cross sectional size, we show in figure 2 the relaxation strain for a $L = 6$ nm long ⟨100⟩/{100} nanowire where the side length D varies between 2 and 3 nm. In this case, we demonstrate that the larger cross section, the smaller the relaxation strain for a given electric field intensity. This result, combined with that in figure 1 demonstrates that the relaxation strain for the nanowire for a given electric field increases nonlinearly with increasing electric field strength, and is dependent on both the axial length L and side length D, and thus the aspect ratio L/D.

We also consider nanowires with the same geometry, but different surface and axial orientations. For this, we consider a nanowire geometry that is $10 \times 2 \times 2$ nm^3, with four

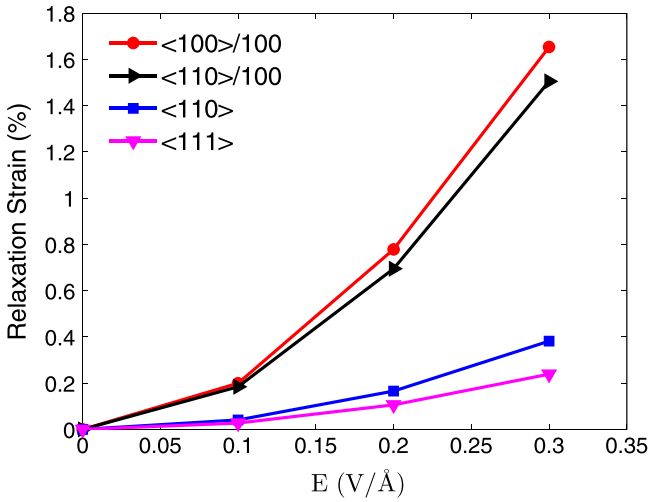

Figure 3. The relaxation strain for a $10 \times 2 \times 2$ nm^3 silver nanowire under increasing electric field intensity. The four nanowires considered are ⟨100⟩/{100}, ⟨100⟩/{110}, ⟨110⟩ and ⟨111⟩.

different configurations: ⟨100⟩/{100}, ⟨100⟩/{110}, ⟨110⟩ and ⟨111⟩. The relaxation strains for these four nanowires under different electric field intensities are shown in figure 3. As shown in figure 3, the ⟨100⟩/{100} and ⟨100⟩/{110} nanowires show the largest relaxation strains with the strains for the ⟨100⟩/{110} nanowire being slightly smaller. In contrast, the ⟨110⟩ and ⟨111⟩ nanowires exhibit considerably smaller relaxation strains for the same electric field intensity. In comparing the two ⟨100⟩ nanowires with different surface orientations, the relaxation strain is higher for the {100} surface than the {110} surface, which is likely due to the higher density of atoms on the {100} surface that can interact with the electric field.

However, we still need to explain why the relaxation strain for the ⟨100⟩ nanowires is larger than the ⟨110⟩ nanowires, which is finally larger than the ⟨111⟩ nanowires. The reason for this lies in the distance between adjacent planes along the axial direction. For example, for the ⟨100⟩ nanowires, the distance between atomic planes along the ⟨100⟩ direction is $a/2$, where $a = 4.09$ Å is the lattice constant for silver. In contrast, the distance between atomic planes in the ⟨110⟩ direction is $\sqrt{2}\,a/2$, while in the ⟨111⟩ direction it is $2\sqrt{3}\,a/3$. This interplanar distance determines how strongly the atoms interact with each other under the effect of the applied electric field, and explains the trend in the relaxation strain for different axial orientations seen in figure 3.

4.2. Electric field effects on nanowire Young's modulus

Having characterized the equilibrium configurations due to externally applied electric fields, we now continue to characterize the resulting change in elastic properties. We first consider again the ⟨100⟩/{100} nanowire with dimensions $10 \times 2 \times 2$ nm^3, subject to tensile loading under electric fields ranging from 0 to 0.3 V Å^{-1}.

As shown in figure 4, the stiffness of the nanowire increases steadily with increasing electric field, which

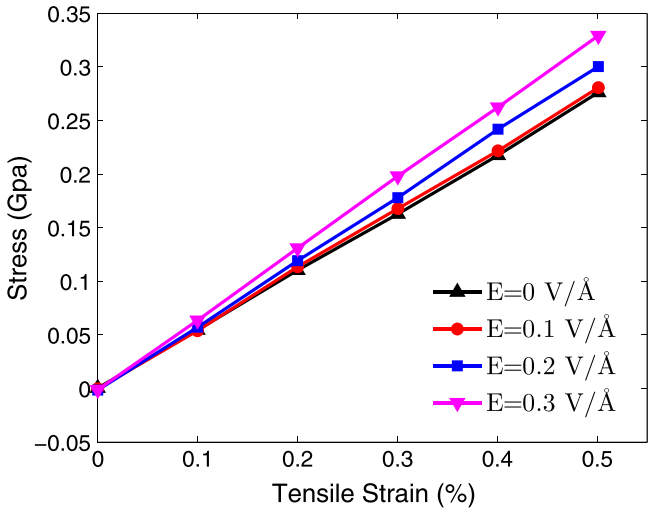

Figure 4. Tensile stress versus strain curve for a $10 \times 2 \times 2\ \text{nm}^3$ ⟨100⟩/{100} silver nanowire, for various electric field intensities ranging from 0 to 0.3 V Å^{-1}, and a maximum tensile strain of 0.5%.

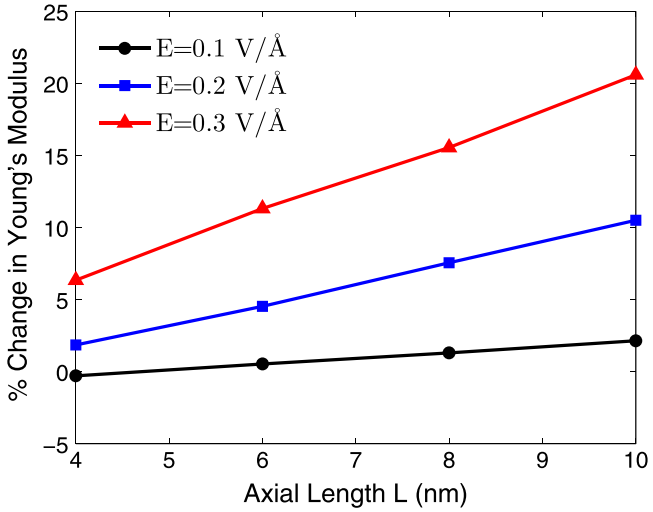

Figure 5. The relative change in the Young's modulus for ⟨100⟩/{100} nanowires with fixed side length $D = 2$ nm, and varying axial lengths of $L = 4$, 6, 8, 10 nm under electric fields with magnitudes 0.1, 0.2, 0.3 V Å^{-1}.

correlates to the increased sensitivity in the form of a larger tensile relaxation strain previously seen in figure 1 as the electric field intensity is increased. In the following, we discuss how size, aspect ratio, surface orientation, and axial orientation, impact the elastic properties of the metal nanowires that are subject to an external electric field.

4.2.1. Axial length effects. We first examine how the Young's modulus is impacted by increasing the aspect ratio of the nanowires as they are subject to different electric field intensities. The percent change in Young's modulus that is plotted in figure 5 and subsequent figures is calculated as $(E - E_0)/E_0$, where E is the Young's modulus of the nanowire subject to electric fields, and E_0 is the Young's modulus of the nanowire without electric field effects. As shown in figure 5 for a ⟨100⟩/{100} nanowire with cross

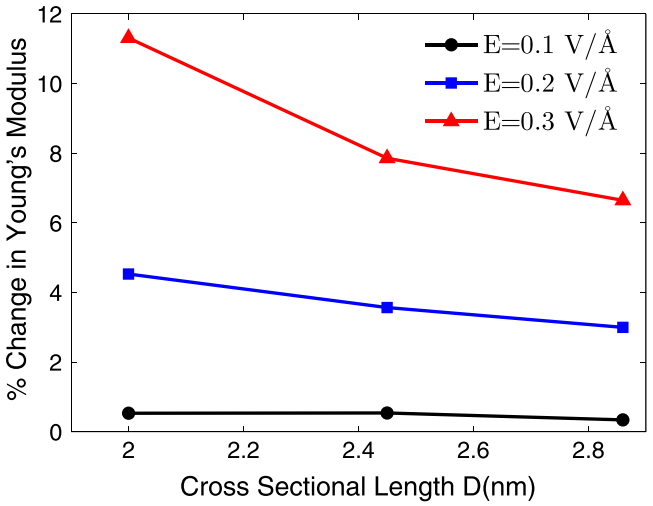

Figure 6. The relative change in the Young's modulus for ⟨100⟩/{100} nanowires with fixed axial length $L = 6$ nm, and varying side lengths $d = 2$, 2.45, 2.86 nm under electric fields of magnitude 0.1, 0.2, 0.3 V Å^{-1}.

sectional dimensions of $2 \times 2\ \text{nm}^2$ and different lengths, the Young's modulus increases with increasing axial length, therefore increasing aspect ratio, and also for increasing electric field intensity. This observation is also found for the other nanowire orientations we considered.

4.2.2. Cross-sectional length effects. We next consider the effects of cross sectional length D on the Young's modulus. In this case, we considered a ⟨100⟩/{100} nanowire with fixed axial length $L = 6$ nm, while varying the cross sectional length D between 2 and 3 nm. As shown in figure 6, as the nanowire thickness increases, the change in nanowire Young's modulus decreases, indicating a weakening of the electric field impact for nanowires with smaller aspect ratios.

4.2.3. Axial orientation and surface effects. Having examined different geometric effects on how electric fields impact the Young's modulus of silver nanowires, we now discuss how the mechanical stiffness of nanowires with different axial orientations, as well as how nanowires with different transverse surfaces are impacted by an externally applied electric field. To do so, we consider the four structures previously discussed, i.e. ⟨100⟩/{100}, ⟨100⟩/{110}, ⟨110⟩, ⟨111⟩. For all four cases, we study silver nanowires with a constant cross sectional length of $D = 2$ nm, while varying the axial length L from 4 to 10 nm to ensure that the difference in Young's modulus induced by the electric field is not due to cross sectional size effects.

The results for the different nanowires are shown in figure 7. As can be seen, with the increasing aspect ratio, both ⟨100⟩ nanowires stiffen while the ⟨110⟩ nanowires soften, under the electrostatic field. In contrast, the ⟨111⟩ nanowires show little change in stiffness with increasing aspect ratio. Indeed, for the purely mechanical case, it was established by Liang *et al* [32] for very small cross section nanowires like the ones considered in this work that bulk nonlinear elasticity,

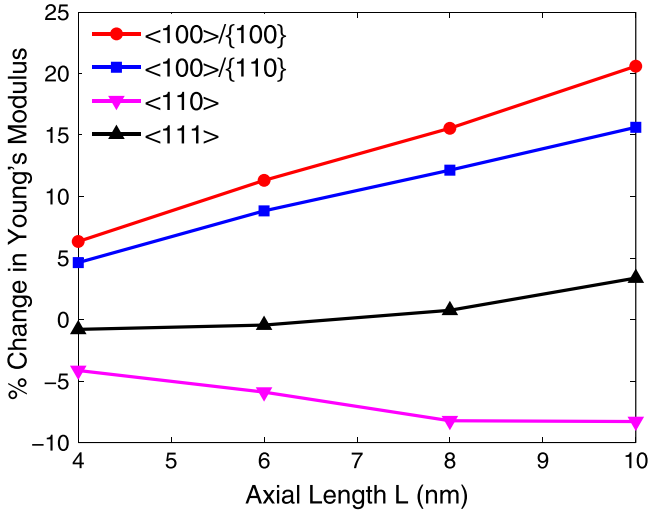

Figure 7. The percentage change in the Young's modulus for nanowires versus the axial length under tensile loading. The electric field magnitude is 0.3 V Å^{-1}, and four different orientations are illustrated. The nanowire side length D = 2 nm while the axial lengths L vary from 4 to 10 nm.

which results from the large compressive strains that nanowires undergo due to the tensile surface stresses [30], causes ⟨100⟩ nanowires to soften as compared to the bulk material, ⟨110⟩ nanowires to stiffen as compared to the bulk material, while ⟨111⟩ nanowires have a relatively small relaxation strain, and thus little change in the mechanical stiffness as compared to the bulk material. Furthermore, the higher the surface-stress-induced compressive strain, the stronger the softening or stiffening effect.

However, when an electric field is applied to the nanowires, the relaxation strain is tensile, as shown in figure 3, and so the nanowire is longer as compared to the mechanically relaxed nanowire, i.e. the nanowire undergoes less compressive strain. Because of this, the compressive bulk nonlinear elasticity that controls the mechanical stiffening or softening in the purely mechanical case [32] is obviated under the electric field, and the nonlinear elasticity-induced stiffening or softening effect that results from the surface-stress-induced compressive strain is weakened. Therefore, compared to the purely mechanical case, the ⟨100⟩ nanowires under electrostatic field have a smaller compressive relaxation strain, which weakens the softening effect and thus results in a higher Young's modulus, while the opposite trend is seen for ⟨110⟩ nanowires. As the nanowire aspect ratio increases, the compressive relaxation strain becomes smaller, and thus a larger relative change in Young's modulus is observed. Again we emphasize that the normalizing value for the Young's modulus E_0 in figure 7 is not the Young's modulus for bulk silver, but the value of purely mechanically stretched nanowire [32].

This also explains the results seen previously in figures 5 and 6. In particular, as shown by Park and Klein [22], the relaxation strain of the nanowires increases with increasing aspect ratio, for a fixed cross sectional size, and decreases with increasing cross sectional size for a constant length. Because the compressive relaxation strain, which increases with increasing length (or increasing aspect ratio), is reduced due to the applied electric field, a larger relative change in Young's modulus is observed in figure 5 with increasing length because longer nanowires exhibit more nonlinear elastic stiffening or softening. In contrast, because the aspect ratio decreases for the constant length nanowires as the cross sectional dimension increases, there is a decrease in the alleviation of the nonlinear elastic softening, and thus a decrease in the change of Young's modulus is observed in figure 6.

The results in figure 7 also shed light on the role of surface effects in controlling the Young's modulus under an applied electric field. Specifically, in comparing the Young's modulus for the two ⟨100⟩ nanowires, it is shown that both have the same trend, i.e. an increasing stiffness with increasing aspect ratio. The ⟨100⟩/{100} nanowire is somewhat stiffer than the ⟨100⟩/{110} nanowire, which is due to the fact that the density of atoms on the {100} surface is higher than that on the {110} surface. Thus, we conclude that while the surface orientation does impact the value of the nanowire stiffness when subject to an electric field, the key factor controlling the magnitude of the stiffness change is in fact the distance between atomic planes along the axial direction of the nanowire bulk.

5. Discussion

Before closing, we compare our atomistic results against those previously obtained using analytical models. In particular, we compare our results against those of Zhu and Zheng [16]. In that work, the authors developed a continuum surface elasticity model incorporating surface electrostatic effects to study the change in the axial and transverse stiffness of copper nanowires due to applied electric fields. For ⟨100⟩/{100} copper nanowires subject to axially applied electric fields, they found a decrease in the axial stiffness of the nanowire. We further note that only ⟨100⟩ nanowires were considered, and thus no orientation-dependency was obtained.

The softening results reported by Zhu and Zheng [16] are in contrast to those we find using the fully coupled electromechanical atomistic model. The reason for this is because the initial relaxation strain, which we capture in this work, and which has previously been established to control the trend of the axial stiffness due to nonlinear elastic effects [32], was not considered in the theoretical model. In other words, the important effect of core nonlinear elasticity is neglected in the theoretical model due to the lack of initial relaxation strain.

6. Conclusion

In conclusion, we have demonstrated, using an electromechanically coupled atomistic simulation with realistic models for both the mechanical and electrostatic properties, that applied electric fields can significantly alter the Young's modulus of metal nanowires. While the effect is most

dramatic for ⟨100⟩ nanowires, ⟨110⟩ and ⟨111⟩ nanowires also show effects, particularly as the aspect ratio increases. The effect appears size-dependent and thus most important for nanowires with very small cross sectional dimensions or high aspect ratios due to the fact that the mechanism underpinning the change in the Young's modulus is the reduction of the nonlinear elastic stiffening or softening that occurs due to the initial surface-stress-induced compressive strain in the relaxed nanowires.

Acknowledgments

XB and HSP both acknowledge the support of the Mechanical Engineering department at Boston University. Both authors also acknowledge the assistance of Prof Lasse Jensen with the point dipole model formulation and parametrization.

References

[1] Lieber C M and Wang Z L 2007 Functional nanowires *MRS Bull.* **32** 99–108
[2] Xia Y, Yang P, Sun Y, Wu Y, Mayers B, Gates B, Yin Y, Kim F and Yan H 2003 One-dimensional nanostructures: synthesis, characterization, and applications *Adv. Mater.* **15** 353–89
[3] Park H S, Cai W, Espinosa H D and Huang H 2009 Mechanics of crystalline nanowires *MRS Bull.* **34** 178–83
[4] Khang D Y, Jiang H, Huang Y and Rogers J A 2006 A stretchable form of single-crystal silicon for high-performance electronics on rubber substrates *Science* **311** 208–12
[5] Rogers J A, Someya T and Huang Y 2010 Materials and mechanics for stretchable electronics *Science* **327** 1603–7
[6] Craighead H G 2000 Nanoelectromechanical systems *Science* **290** 1532–5
[7] Ekinci K L and Roukes M L 2005 Nanoelectromechanical systems *Rev. Sci. Instrum.* **76** 061101
[8] Eom K, Park H S, Yoon D S and Kwon T 2011 Nanomechanical resonators and their applications in biological/chemical detection: nanomechanics principles *Phys. Rep.* **503** 115–63
[9] Zheng X and Zhu L 2006 Theoretical analysis of electric field effect on Young's modulus of nanowires *Appl. Phys. Lett.* **89** 153110
[10] Huang Y, Bai X and Zhang Y 2006 *In situ* mechanical properties of individual ZnO nanowires and the mass measurement of nanoparticles *J. Phys.: Condens. Matter.* **18** L179–84
[11] Chen C Q, Shi Y, Zhang Y S, Zhu J and Yan Y J 2006 Size dependence of the Young's modulus of ZnO nanowires *Phys. Rev. Lett.* **96** 075505
[12] Bernal R A, Agrawal R, Peng B, Bertness K A, Sanford N A, Davydov A V and Espinosa H D 2010 Effect of growth orientation and diameter on the elasticity of GaN nanowires. A combined *in situ* TEM and atomistic modeling investigation *Nano Lett.* **11** 548–55
[13] Zijlstra P, Tchebotareva A L, Chon J W M, Gu M and Orrit M 2008 Acoustic oscillations and elastic moduli of single gold nanorods *Nano Lett.* **8** 3493–7
[14] Purcell S T, Vincent P, Journet C and Binh V T 2002 Tuning of nanotube mechanical resonances by electric field pulling *Phys. Rev. Lett.* **89** 276103
[15] Sapmaz S, Blanter Y M, Gurevich L and Van der Zant H S J 2003 Carbon nanotubes as nanoelectromechanical systems *Phys. Rev.* B **67** 235414
[16] Zhu L and Zheng X 2010 Modification of the elastic properties of nanostructures with surface charges in applied electric fields *Eur. J. Mech.* A **29** 337–47
[17] Wang Z, Devel M, Langlet R and Dulmet B 2007 Electrostatic deflections of cantilevered semiconducting single-walled carbon nanotubes *Phys. Rev.* B **75** 205414
[18] Wang Z and Devel M 2007 Electrostatic deflections of cantilevered metallic carbon nanotubes via charge-dipole model *Phys. Rev. Lett.* **76** 195434
[19] Wang Z, Zu X, Yang L, Gao F and Weber W J 2007 Atomistic simulation of the size, orientation, and temperature dependence of tensile behavior in GaN nanowires *Phys. Rev.* B **76** 045310
[20] Wang Z and Philippe L 2009 Deformation of doubly clamped single-walled carbon nanotubes in an electrostatic field *Phys. Rev. Lett.* **102** 215501
[21] Foiles S M, Baskes M I and Daw M S 1986 Embedded-atom-method functions for the fcc metals Cu, Ag, Au, Ni, Pd, Pt, and their alloys *Phys. Rev.* B **33** 7983–91
[22] Park H S and Klein P A 2007 Surface Cauchy–Born analysis of surface stress effects on metallic nanowires *Phys. Rev.* B **75** 085408
[23] Wan J, Fan Y L, Gong D W, Shen S G and Fan X Q 1999 Surface relaxation and stress of fcc metals: Cu, Ag, Au, Ni, Pd, Pt, Al and Pb *Modelling Simul. Mater. Sci. Eng.* **7** 189–206
[24] Jensen L L and Jensen L 2008 Electrostatic interaction model for the calculation of the polarizability of large nobel metal nanostructures *J. Phys. Chem.* C **112** 15697–703
[25] Payton J L, Morton S M, Moore J E and Jensen L 2012 A discrete interaction model/quantum mechanical method for simulating surface-enhanced Raman spectroscopy *J. Phys. Chem.* **136** 214103
[26] Purcell E M and Pennypacker C R 1973 Scattering and absorption of light by nonspherical dielectric grains *Astrophys. J.* **1986** 705–14
[27] Johnson P B and Christy R W 1972 Optical constants of the noble metals *Phys. Rev.* B **6** 4370–9
[28] Lammps 2013 http://lammps.sandia.gov/
[29] Cammarata R C 1994 Surface and interface stress effects in thin films *Prog. Surf. Sci.* **46** 1–38
[30] Park H S, Gall K and Zimmerman J A 2005 Shape memory and pseudoelasticity in metal nanowires *Phys. Rev. Lett.* **95** 255504
[31] Diao J, Gall K and Dunn M L 2003 Surface-stress-induced phase transformation in metal nanowires *Nat. Mater.* **2** 656–60
[32] Liang H, Upmanyu M and Huang H 2005 Size-dependent elasticity of nanowires: nonlinear effects *Phys. Rev.* B **71** 241403